

# NWP SAF

## *Satellite Application Facility for Numerical Weather Prediction*

Document NWPSAF-MO-VS-011

Version 1.0

15 April 2006

## Quantitative precipitation estimation from satellite data

Sante Laviola

University of Basilicata, Potenza-Italy



# Quantitative precipitation estimation from satellite data

Sante Laviola

University of Basilicata, Potenza-Italy

This documentation was developed within the context of the EUMETSAT Satellite Application Facility on Numerical Weather Prediction (NWP SAF), under the Cooperation Agreement dated 16 December, 2003, between EUMETSAT and the Met Office, UK, by one or more partners within the NWP SAF. The partners in the NWP SAF are the Met Office, ECMWF, KNMI and Météo France.

**Copyright 2006, EUMETSAT, All Rights Reserved.**

## **Acknowledgement**

This work was performed during a 6 months visiting scientists of Sante Laviola, PhD student at University of Basilicata (Potenza-Italy), at Met Office (UK) within the framework of EUMETSAT's Numerical Weather Prediction Satellite Application Facility (SAFNWP).

## Abstract

In the present paper I will describe the work carried out during six months visit at Met Office (UK). The aim of this work has been to study and possibly improve the Bennartz method to remotely estimate precipitation affecting the satellite signal in the microwave spectral region.

Bennartz algorithm, based on the AMSU high frequencies, is able to detect and classify the precipitation intensity over water, coast and land surfaces. By using the scattering effect at 89 GHz and 150 GHz due to the growing ice crystals in upper part of the clouds, the scattering index gives a measure strictly linked to the surface precipitation. Therefore, four different classes of precipitation intensities are used: precipitation-free, risk of precipitation, light or moderate rain and heavy rain (> 5 mm/h).

In 2000 Grody et al. developed a series of algorithms to retrieve geophysical parameters using thresholds to derive hydrological parameters and remove surface feature effects as snow cover and sea ice contaminating precipitation estimation.

Qualitative and quantitative comparisons between Grody and Bennartz algorithms have shown as the Bennartz technique is more sensitive to the presence of rainy clouds than Grody showing a high correlation with the radar data particularly on the heavily rain areas. Nevertheless, AMSU-B window channels are largely dependent on the atmospheric conditions over ocean surface, so the algorithm predictions can overestimate or underestimate the amount of precipitation. To reduce the ambiguities and improve the retrieval method, RTTOVSCATT with 20000 ECMWF diverse profiles over ocean as input data has been used. The scattering index with synthetic data increases with increasing of Cloud Liquid Water (CLW) giving values comparables with precipitation signature. At the end of this study, a new offset brightness temperature for water surface is computed.

# Contents

<b>1. Introduction</b>	<b>4</b>
<b>2. Dataset</b>	
2.1 The Advanced Microwave Sounding Unit	5
2.2 Satellite and Radar Data	6
2.3 Synthetic Data	6
<b>3. Scattering Index Approach</b>	
3.1 Water Surface	8
3.1.1 Emission Signal	8
3.1.2 Scattering Signal	8
<b>4. Bennartz and Grody Algorithms</b>	<b>8</b>
4.1 Qualitative Comparison	9
4.2 Quantitative Comparison	11
<b>5. Algorithm Improvement</b>	<b>15</b>
<b>6. Summary and Conclusions</b>	<b>21</b>

# 1. Introduction

Precipitation is an important key in the climate sciences and its role is fundamental from the large scale to the smaller. When water evaporates, heat is absorbed from the environment; the condensation of the water vapour in liquid or ice particles releases latent heat in surrounding air warming it. Two different types of precipitation with respect to physical mechanisms which generate rain particles can be observed. In the upper part of the clouds where the temperatures are typically around  $-20^{\circ}\text{C}$ , ice crystals and supercooled liquid water particles can coexist. Because the saturation vapour pressure is greater over water liquid particles than over ice, water vapour migrates from supercooled water to the ice crystals rapidly growing. The “warm” mechanism is based on the coalescence phenomenon, droplets collide and coalesce, further increasing the range of size and fall velocity. In the last years, an accurate monitoring of precipitation events was carried out with different kinds of instruments which are of potential interest for the remote sensing of rainy clouds. Visible and Infrared sensors such as the Advanced Very High Resolution Radiometer (AVHRR) and microwave instruments such as the Advanced Microwave Sounding Unit (AMSU). Although AVHRR sounds the atmosphere to very high resolution (in the order of 1 km at nadir), the electromagnetic radiation emitted towards the satellite view is largely extinguished from the rainy clouds so that it can not be distinguish between cold thick clouds with or without precipitation and all information has to be derived from indirect measures such as cloud optical properties or cloud top temperature.

Microwave radiation fields are directly influenced from the signatures of precipitating systems giving a direct measures of precipitation. The atmospheric particles, liquid water droplets and ice crystals, emit, absorb and scatter at microwave frequencies. The drawback of the passive microwave instruments is their low spatial resolution of typically several  $10^{\text{th}}$  of kilometres.

Microwave instruments are used to measure both atmospheric and surface parameters under all weather conditions. Grody et al. [1] have developed a complete series of algorithms, initially proposed for SSM/I and successively fit to the AMSU sensor, to measure water vapour, cloud liquid water and precipitation rates, snow cover and sea ice concentration with different spatial resolution. By using mainly, AMSU-B water vapour absorption channels around 183.3 GHz, Staelin D. and Chen F. [2] develop a neural network algorithm, based on NEXRAD data, able to estimate precipitation rates on AMSU high resolution.

Recently, rainfall downscaling models, have been implemented to disaggregate the large scale rainfall forecast into smaller scales for hydrological catchment models [3] [4]. The improvement of the procedures to fill the existing gap between the large scales in space and time to which meteorological models work and the small scales that are required by hydrological rainfall-runoff modelling.

At U. K. Meteorological Office (UKMO) a new method to identify precipitation and classify its intensities over water, land and coast surfaces from AMSU-B data is used [5].

The scattering index approach which the Bennartz technique is based on, works by using the scattering signal at 89 GHz and 150 GHz. The variations to the passive microwave radiation are generally strictly correlated to the amount of precipitation even if the relation between surface rain rate and observed brightness temperatures is difficult to establish. The brightness temperature depression due to the interaction with cold thick cloud is largely caused by the precipitation size of ice particles. At high frequencies these large ice crystals scatter cold radiation back to the satellite.

In present report I will describe some qualitative and quantitative comparisons between the Grody and Bennartz algorithms and radar data. A improvement of the Bennartz technique over ocean is introduced, reducing the effect of cloud liquid water on the scattering index.

## 2. Dataset

### 2.1 The Advanced Microwave Sounding Unit

The AMSU cross-track scanning sensor consists of two independent instruments: AMSU-A and AMSU-B modules. AMSU-A instrument, composed of two separate modules A1 and A2 have the 15 lower frequency channels (23.8 – 89.0 GHz) primarily for temperature sounding from the surface to 2 hPa. AMSU-A has a nominal field of view of 3.3° (45 km on surface at nadir) being able to obtain 30 measurements along each scan line, covering nearly 2300 km swath on Earth. The A1 module has 12 channels in the oxygen band and provides information on the temperature profile, whereas A2 module has two channels which are primarily used to derive non-sounding products. AMSU-A four window frequencies are used to detect the surface features.

The main purpose of the AMSU-B package is the retrieval of water vapour profile information up to 200 hPa. The AMSU-B is a five high frequency channels two are centred nominally at 89 GHz and 150 GHz, and the other three are around 183.31 GHz water vapour line with double sideband centres located at 183.31+/-1, +/-3 and +/-7 GHz, respectively. AMSU-B FOV is of 1.1° degrees +/- 10 % and once every 8/3 seconds it measures 90 Earth views, four space views and four internal blackbody target views. The satellite viewing angle for the innermost scan positions is +/-0.55° from nadir, for the outermost scan positions it is +/-48.95°. The footprint size is 20x16 km<sup>2</sup> of the innermost scan position, but increase to 64x27 km<sup>2</sup> for the outermost positions. All AMSU channel characteristics are pointed out in Table 1.

AMSU-A :										
Channel Number	Channel Frequency (MHz)	Number of Bands	Measured 3-dB Bandwidth (MHz)	NEAT Spec. (K)	Measured (K)	Main Beam Efficiency	Cross Polarization Beam Efficiency	3-dB Beamwidth (deg.) **	Polarization at nadir	Remarks
1	23900	1	251.02	0.30	0.211	95.39%	1.57%	3.53	V	A2/PFM
2	31400	1	161.20	0.30	0.265	97.14%	1.23%	3.41	V	"
3	50300	1	161.14	0.40	0.219	95.39%	2.24%	3.76	V	A1-2/FM1
4	52800	1	390.52	0.25	0.143	95.50%	1.21%	3.72	V	"
5	53596 ± 115	2	168.20	0.26	0.148	95.55%	1.38%	3.70	H	"
6	54400	1	390.54	0.25	0.154	95.08%	1.65%	3.68	H	A1-1/FM1
7	54940	1	390.56	0.25	0.132	94.79%	1.47%	3.61	V	"
8	55500	1	310.34	0.25	0.141	95.05%	1.44%	3.63	H	A1-2/FM1
9	f <sub>0</sub> = 57290.344	1	310.42	0.25	0.236	95.91%	1.29%	3.51	H	A1-1/FM1
10	f <sub>0</sub> ± 217	2	76.58	0.40	0.250	"	"	"	H	"
11	f <sub>0</sub> ± 322.2 ± 48	4	35.11	0.40	0.280	"	"	"	H	"
12	f <sub>0</sub> ± 322.2 ± 22	4	15.29	0.60	0.400	"	"	"	H	"
13	f <sub>0</sub> ± 322.2 ± 10	4	7.93	0.80	0.539	"	"	"	H	"
14	f <sub>0</sub> ± 322.2 ± 4.5	4	2.94	1.20	0.914	"	"	"	H	"
15	89000	1	1998.98	0.50	0.166	97.79%	1.38%	3.80	V	"
** Specification is required to have 3.3 degrees ± 10% for all channels.										
AMSU-B :										
16	89000	2	1000	1.0	0.37	94.4%	0.2%	1.12	V	PFM
17	150000	2	1000	1.0	0.84	95.1%	1.4%	1.08	V	PFM
18	183310 ± 1000	2	500	1.0	1.06	96.9%	0.8%	1.12	V	PFM
19	183310 ± 3000	2	1000	1.0	0.70					
20	183310 ± 7000	2	2000	1.2	0.60					

Table 1: Channel characteristics and specifications of AMSU instruments

In the presence of a precipitation signatures AMSU frequency response is completely different. Generally, liquid water drops affect mostly low frequency channels (23.8 and 31.4 GHz) showing a warm signal over a cold target, as ocean. The high variation of the surface emissivity, particularly over land (on the ocean surface it can range 0.4-0.6), affects strongly microwave natural radiation contaminating the precipitation signature. Therefore, the use of algorithm to filter out the false signal is need [1].

On the contrary, the AMSU-B brightness temperature depression caused by precipitation sized ice crystals, indirectly linked with surface rain, can be observed both over land and over water surfaces [1] [6] [7] [8]. At high frequencies these large ice particles scatter cold radiation above the cloud back to the satellite.

## **2.2 Satellite and Radar Data**

The evaluation of the qualitative and quantitative performances of the Grody and Bennartz techniques were carried out by comparing with radar data. For this study, Met Office Nimrod European composite data on a 5 km resolution grid, covering the UK and Northern parts and Western mainland Europe, were used. The data files are available every 15 minutes and include information on instantaneous rain rate, which should have a direct correlation to the scattering index. In order to compare radar and satellite different spatial resolutions, the weather radar data were averaged to the AMSU-B 16 km grid. Nevertheless, this convolution method of the radar data is not optimal convolution scheme. To implemented this would be time-consuming and would require more time than this project allows. The current averaging will become more inaccurate towards the edge of the satellite scan, where the distance between satellite grid points increase.

The algorithm performances are tested on 20 different orbits ranging from January to December 2004, co-located with radar data and selected from Met Office Data Base.

## **2.3 Synthetic Data**

The synthetic data have been computed by using RTTOVSCATT which simulates both clear and rainy conditions with 20000 ECMWF profiles over ocean as a input. RTTOVSCATT is a version of the radiative transfer model RTTOV with the capability to handle the scattering radiation by hydrometeors by using delta-Eddington approximation. The Eddington approach to scattering approximates the radiance vector and the phase function to the first order so that only one angle is required for the scattering calculations. Marshall-Palmer size distribution function for rain droplets and modified gamma for ice crystals are assumed.

In figures 1 and 2 are the scatter plots of 89 GHz and 150 GHz synthetic data of clear versus rainy conditions; as it can be seen, the rain largely absorbs 89 GHz radiation increasing the brightness temperatures up to 40 K with respect to the clear sky conditions. At 150 GHz precipitation scattering particles depress brightness temperatures of 30 K.

To emphasize the effects for each profile parameter on the scattering index, complete input data were unpacked and AMSU-B brightness temperatures in all single steps were simulated. These results are presented in the section 5.

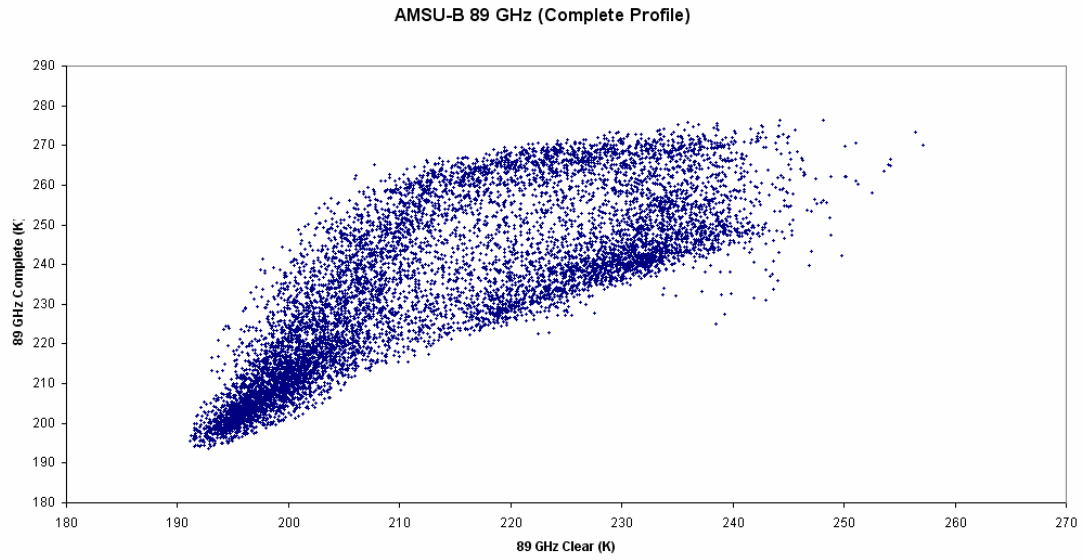


Fig. 1: Scatter plot of 89 GHz clear versus rainy conditions. Complete Profile is the profile with Cloud Liquid Water (CLW), Cloud Ice Water (CIW), Rain, Snow and Convective and Stratiform precipitations

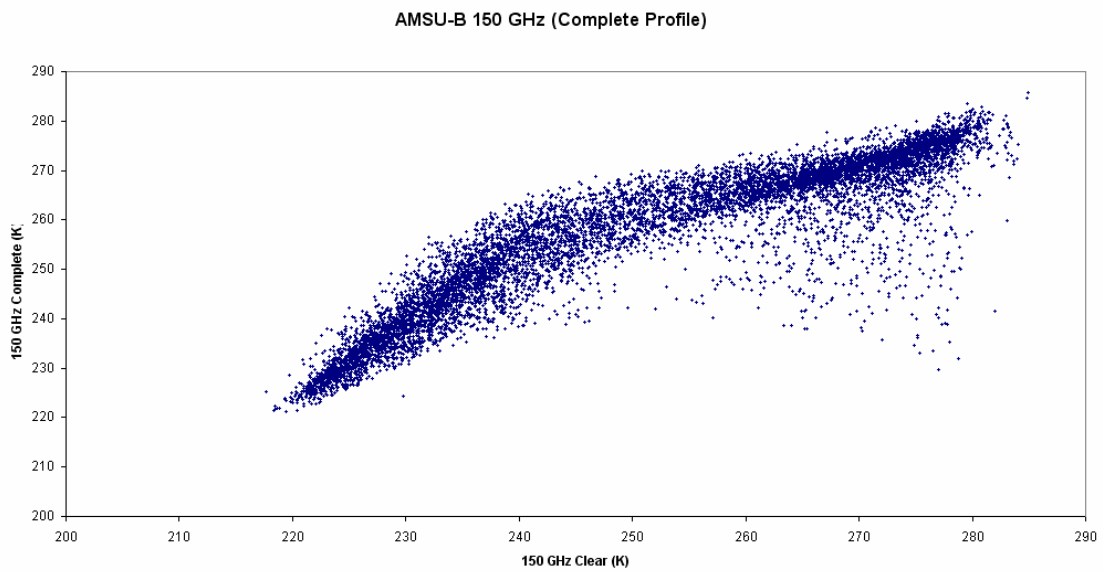


Fig. 2: As above but for 150 GHz

## 3. Scattering Index Approach

### 3.1 Water Surface

The response of passive microwave brightness temperatures to precipitation over water surface is strongly dependent on the water vapour path and atmospheric temperature because the “cold” target background. Two commonly used ways to detect precipitation over ocean are emission and scattering approaches.

#### 3.1.1 Emission Signal

The rain rate is strictly correlated to the increase of the liquid water amount in the clouds. Since large rain droplets lead to a strong increase in optical depth, a rain rate relationship can be obtained by correlating the liquid water measurements against co-located rain gauge and radar measurements [1]. The AMSU-A low frequency channels, for example, can be used to identify situations where liquid water path exceeds a certain thresholds [1] [9]. However, in this study we don't use a cloud liquid water index to compute precipitation signatures but we study the emission signal at 89 GHz due to the CLW affecting the scattering index.

#### 3.1.2 Scattering Signal

As presented in [5], several combinations of window channels are used to obtain scattering indices, in the same way both as for land and for sea surfaces. Although, both the channel at 89 GHz and at 150 GHz one are affected by the scattering, this combination was optimal, with the added advantage of having the same spatial resolution of AMSU-B.

## 4. Bennartz and Grody Algorithms

In the present section, I will briefly describe the Bennartz and Grody algorithms used in this study. Dependent on the AMSU-B footprint can be considered as homogeneous land or also the surrounding AMSU-A footprint, two different algorithms was empirically developed by regressing analysis of the scattering index for all-precipitation free observations against the local zenith angle. Nevertheless, only that for AMSU-B homogeneous land is used.

$$s_{ll} = (T_{89} - T_{150}) - (0.158 + 0.0163\theta) \quad (\text{B1})$$

where  $\theta$  is the zenith angle of the observation.  
For water surface, the Bennartz algorithm is

$$s_{sl} = (T_{89} - T_{150}) - (-39.2010 + 0.1104\theta) \quad (\text{B2})$$

The last term is the least general part of the algorithm since it is supposed to be strongly dependent on the water vapour path and atmospheric temperature and thus may not be valid for different regions. The algorithm used for coast is a mixture of the land and sea equations.

Based on AMSU-A/B data, many different equations to measure rain rates and derive hydrological parameters Grody developed. However, in order to compare to the same spatial resolution of Bennartz algorithm, only the scattering indices on the AMSU-B frequencies have been used. For land and sea surfaces, the Grody equations are respectively the followings:

$$s_{land} = [42.72 + 0.85T_{89}] - T_{150} \quad (G1)$$

$$s_{sea} = 0.013[T_{89} + 33.58 \ln(300 - T_{150}) - 341.17] \quad (G2)$$

For land surface the rain rates exceeding 1 mm/h are identified when the index exceeds a 5 K threshold. Over ocean the index approximates the liquid water amount. Values greater than 0.35 mm was found to discriminate between rain and no-rain condition [1] [5].

## 4.2 Qualitative Comparison

The first evaluation of the scattering index imagery was carried out by a qualitative comparison of the radar data over the UK area with using Met Office Nimrod European composite data.

In figure 3 is reported the comparison of two scattering indices with the radar data for one case study, showing a low pressure to the west of the UK on 22 June 2004. The satellite pass data ranges from 14:02 to 14:08 and the radar data is at 14:00. It can be seen as Grody's results largely overestimate the rainy areas compared to Bennartz. The Bennartz scattering index is capable of producing a qualitative match to the radar rain over land, in terms of spatial extent and relative intensity, however over water surfaces the signal is too weak. The discrepancy between Bennartz data and radar data is due to the use of a fixed brightness temperature offset threshold to estimate the rain over sea.

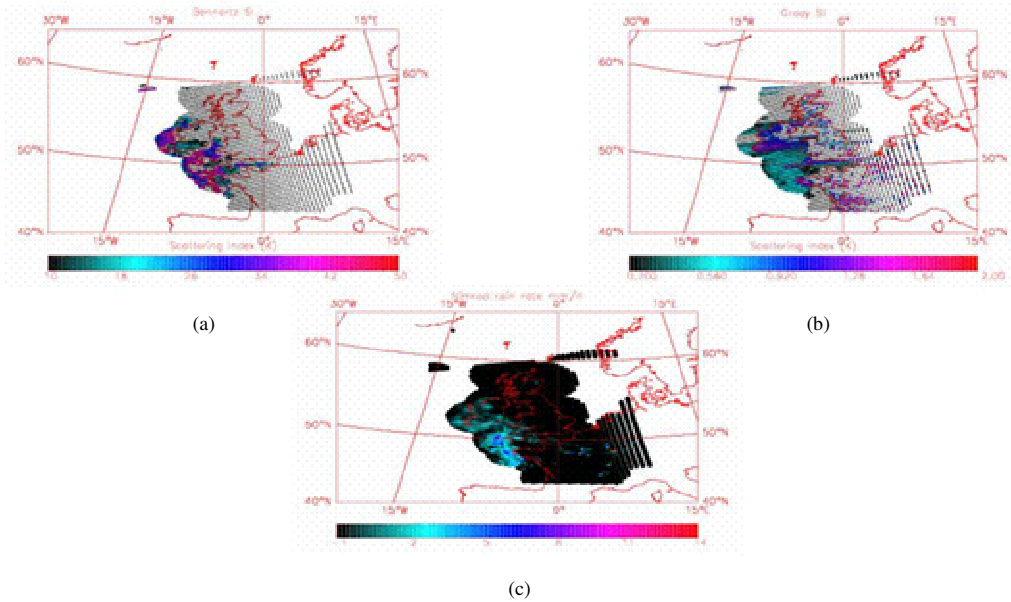


Fig 3: Bennartz and Grody algorithms compared with Nimrod radar data at 1400 on 22/06/04, convolved to the AMSU-B grid, 3-a, 3-b and 3-c respectively

In figure 4 is another case study, 09 August 2004, where the radar precipitation image is associated to the cold front over Ireland and Scotland. Again the Bennartz scattering index estimates precipitation matched to the radar rain over land with respect to the Grody values. This figure also shows up areas of scattering to the south-east of UK, where the radar detects rain. However, over sea among the coast of UK and Ireland rain is not picked out.

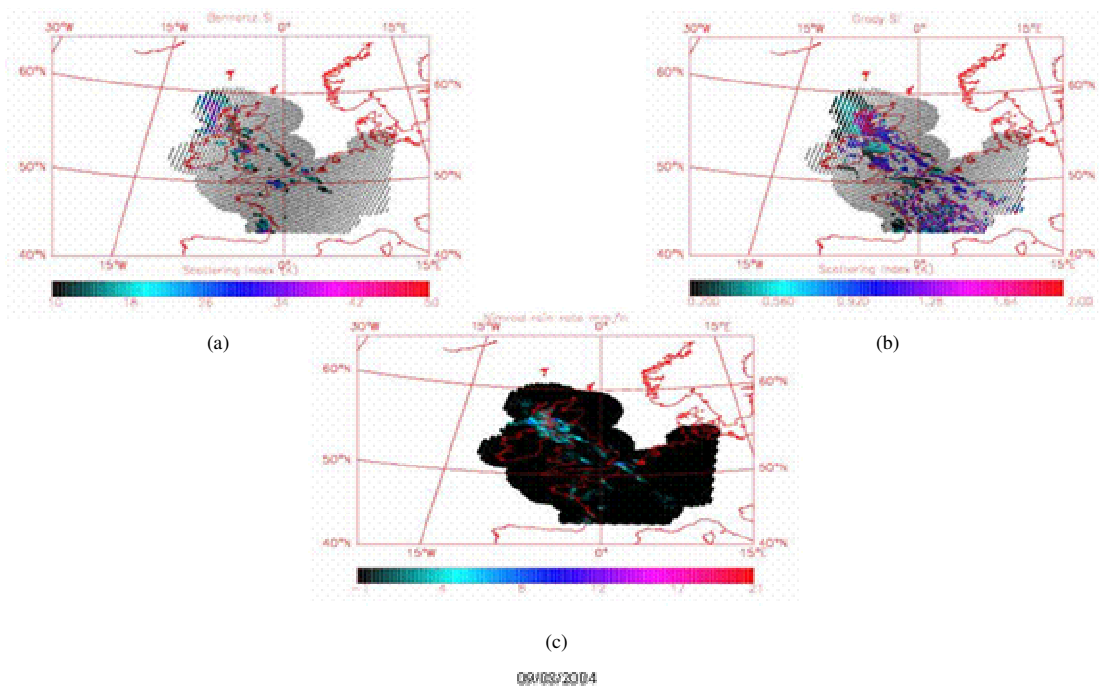


Fig.4: Bennartz and Grody algorithms compared with Nimrod radar data at 0700 on 09/08/04, convolved to the AMSU-B grid, 4-a, 4-b and 4-c respectively

Other comparisons are made in this work, and all of them show as the Grody scattering index overestimates the rain rates compared to Bennartz's results.

### 4.3 Quantitative Comparison

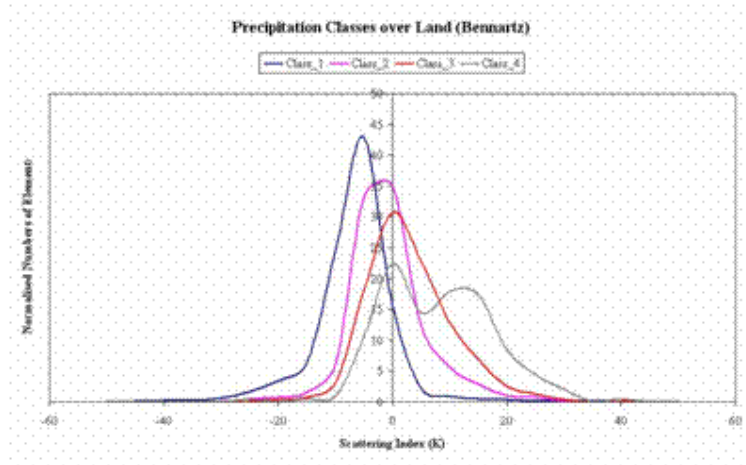
In section 4.2 the best match between Bennartz scattering index with respect to Grody's results and radar precipitation measurements is shown. In the present section, a quantitative comparison is presented.

As the scattering index data represents a probability of precipitation rather than an actual precipitation rate, the quantitative evaluation is based on the ability of the index to represent the four rain rate classes presented in figure 5, which are defined from the convolved rain rate data [5].

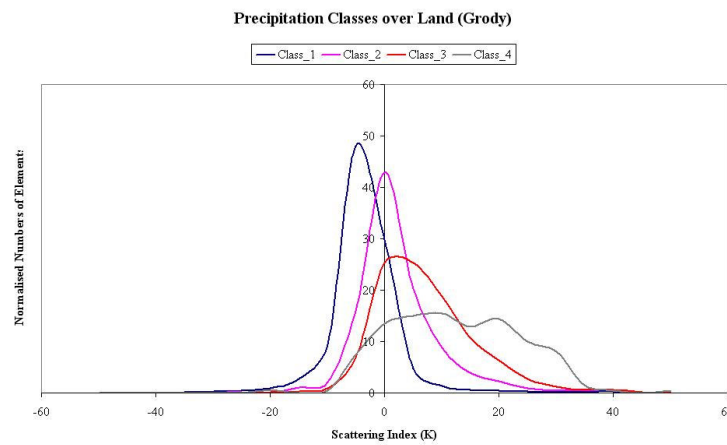
Class	Description	Minimum rain rate (mm/h)	Maximum rain rate(mm/h)
1	No rain	0.0	0.1
2	Risk of light rain	0.1	0.5
3	Light to moderate rain	0.5	5.0
4	Heavy rain	5.0	$\infty$

Fig.5: Classification of precipitation intensities

In the following figures the histograms of the scattering index distributions for the four precipitation classes are presented. The histograms have been normalized by the number of data points in each class in order to give a representation of the prior probability of the rain rate class occurring, as well as the probability of a given scattering index belonging to that class. In figure 6, which depicts the algorithm performances over land surface, it can be seen as the separability of the classes over water surfaces is large in both cases. This reflects the sensitivity of the algorithms to largely discriminate the different intensities of rain. Interestingly, two techniques are strongly sensitive to the risk of light rain and to the moderate precipitation (classes 2<sup>nd</sup> and 3<sup>rd</sup>) compared with 4<sup>th</sup> class (heavy rain). Nevertheless, since the satellite is sensing from a cold atmosphere over a warm surface, more ambiguity may arise due to the high variability of the surface.



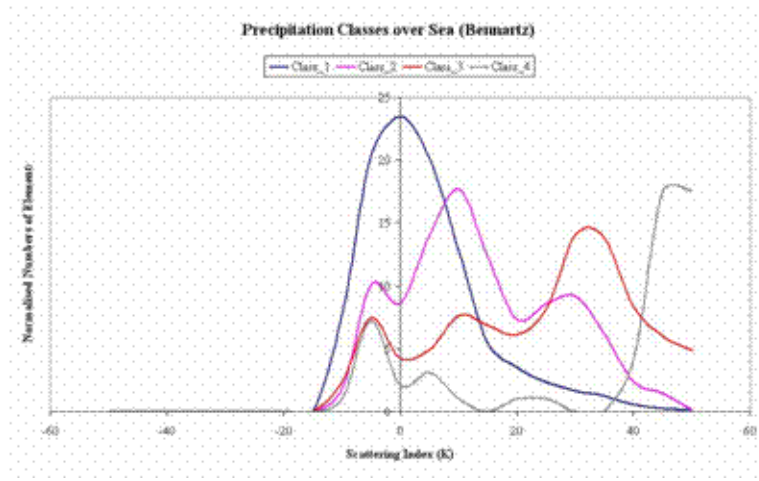
(a)



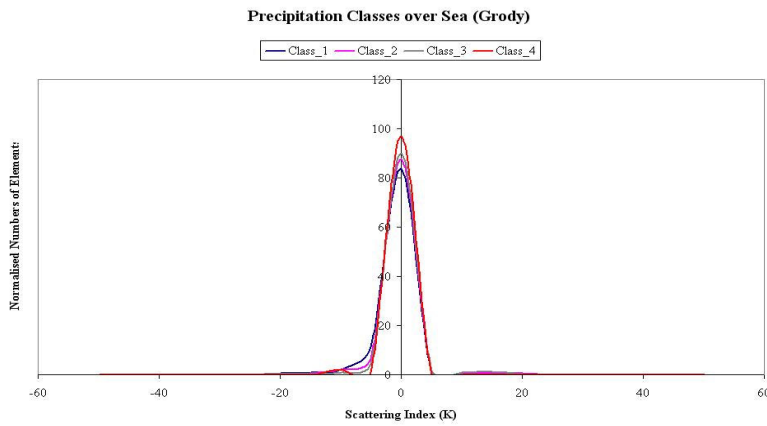
(b)

Fig.6: Histograms (normalised by the number of elements in each class) showing the distribution of the scattering index for the four rain rate classes for land points, 6-a and 6-b Bennartz and Grody algorithms respectively

Over sea surface (figure 7), the Bennartz scattering index is greatly more able than Grody algorithm to discriminate the different types of rain. Although the first three classes are overlapped for low values of the scattering index, a threshold of separability at 20K can be found. In the Grody case, all classes are completely overlapped not giving the possibility to evaluate the intensity of rain.



(a)



(b)

Fig.7: Histograms (normalised by the number of elements in each class) showing the distribution of the scattering index for the four rain rate classes for sea points, 7-a and 7-b Bennartz and Grody algorithms respectively

Figures 8 and 9 show the scatter plot of the Bennartz versus Grody results. Over land, both algorithms are strictly correlated showing a high correlation coefficient ( $S= 0.958$ ). Over sea surface, instead, the correlation is lower than the latter.

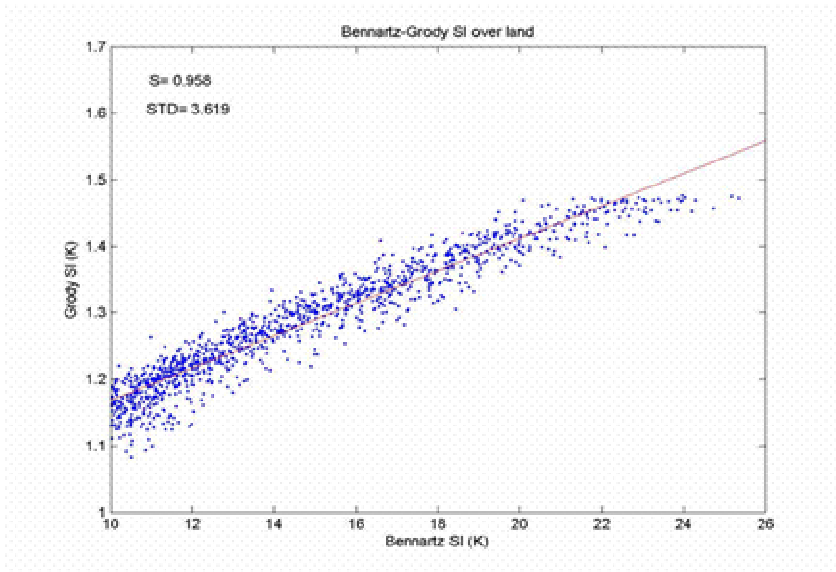


Fig. 8: Scatter plot between Bennartz and Grody algorithms over land surface

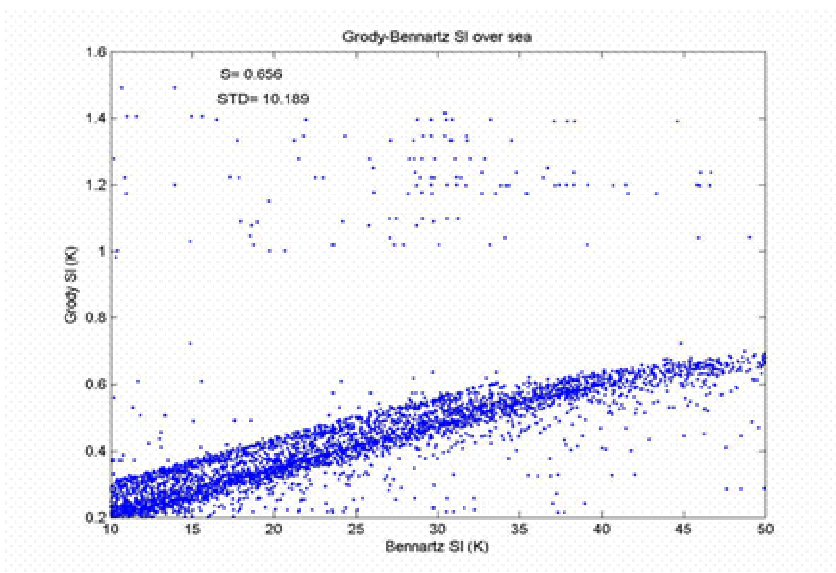


Fig. 9: As above but for sea

## 5. Algorithm Improvement

In this section a new brightness temperature offset for Bennartz equation (B2) is proposed. The aim of the following study is the reduction the cloud liquid water emission signal contaminating the scattering index over a cold background as water surface. However, firstly to correctly evaluate CLW effect, the scattering and absorption signatures of other parameters are computed.

In figure 10 the absorption of radiation at 89 GHz due to the rain drops increases the brightness temperatures up to 30 K compared to the clear sky conditions. All scattering effects of other parameters (compare to figure 1) have been removed in the simulation. At 150 GHz in figure 11, we can observe only a small effect by liquid droplets; the changing in slope is caused by the lifting of the weighting function near colder atmospheric layers. Solid rain particles mainly affect the higher frequency (figures 12-13). Larger scattering power at 150 GHz [7] [8] than 89 GHz depress the brightness temperature up to 30 K.

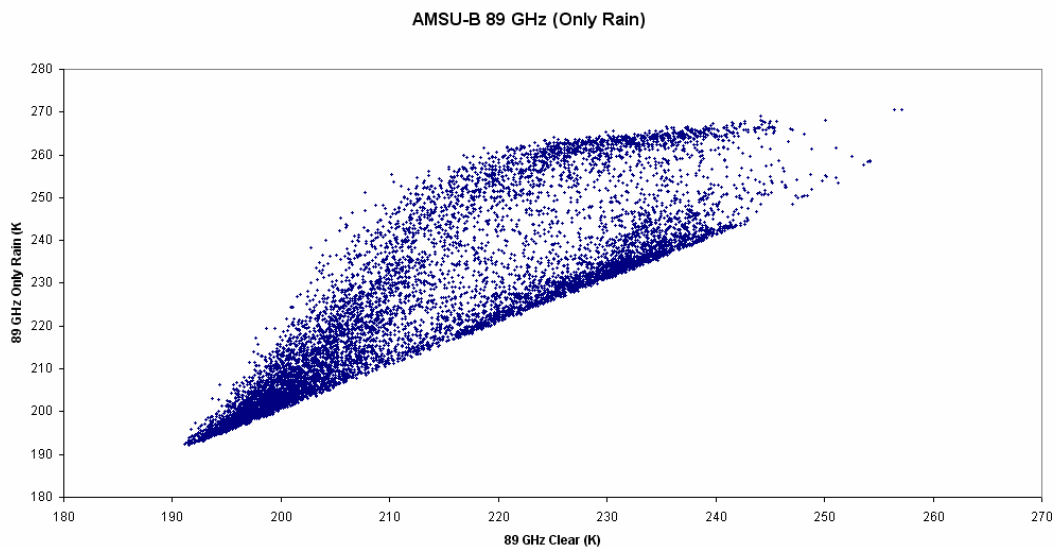


Fig. 10: Effect of liquid rain at 89 GHz. The absorption of liquid rain droplets increase the brightness temperature at 89 GHz up to 40 K

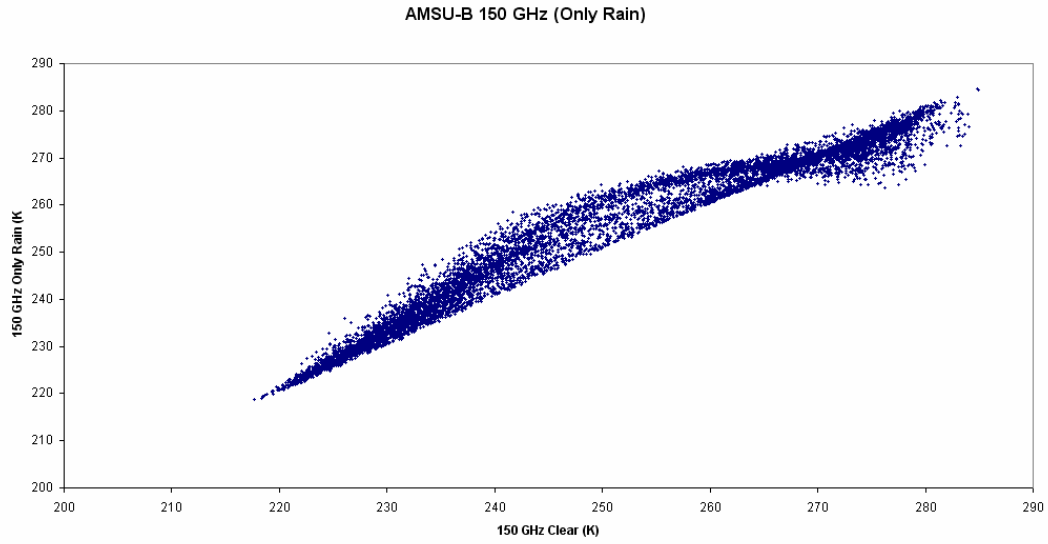


Fig. 11: Effect of liquid rain at 150 GHz. AMSU-B channel 2 is not very absorbing but liquid rain drops lift the weighting function near colder layers

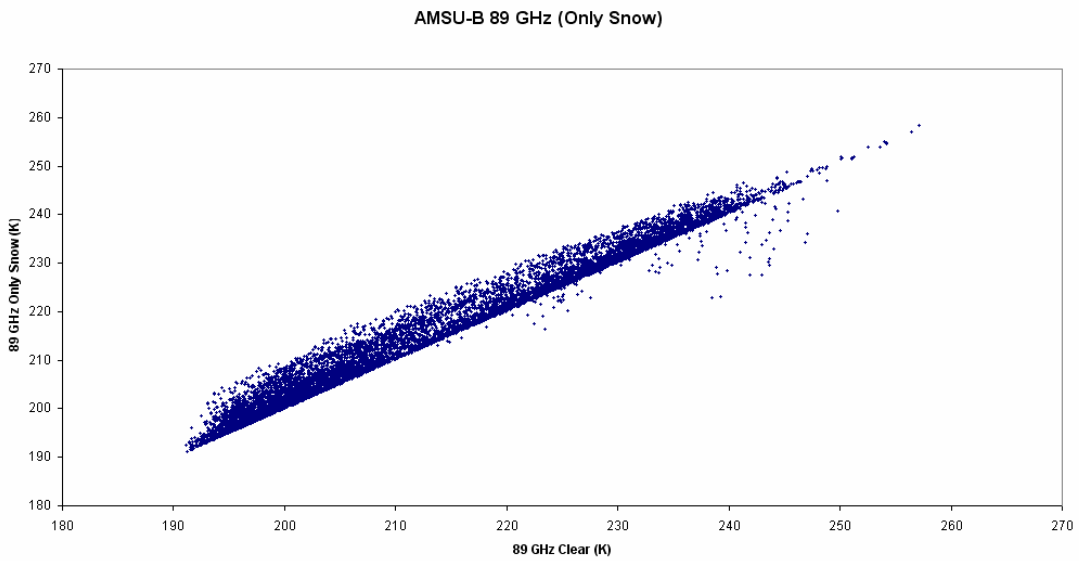


Fig. 12: Effect of snow at 89 GHz. The presence of snow not largely affects the brightness temperatures at 89 GHz

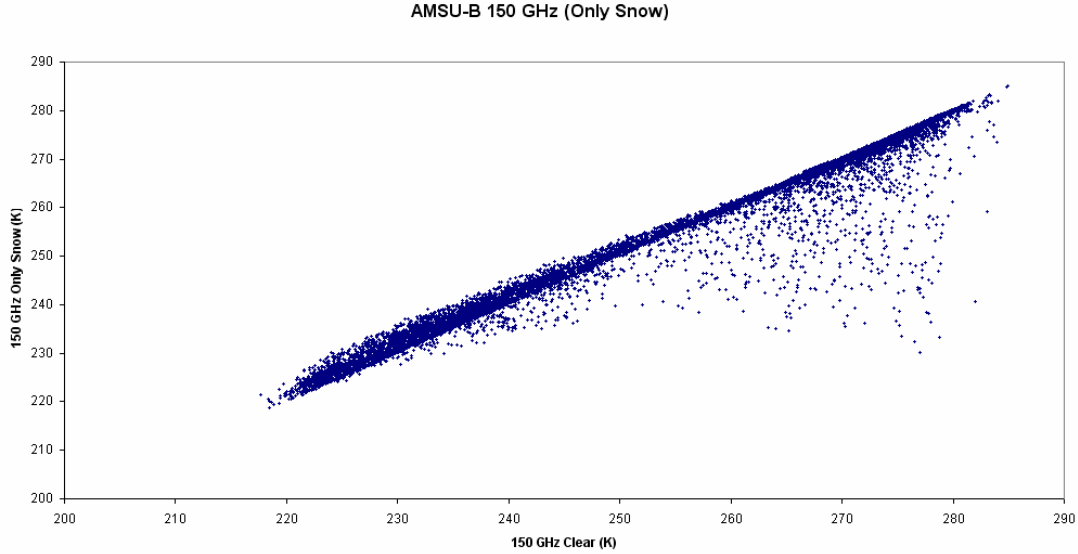


Fig. 13: Effect of snow at 150 GHz. The brightness temperatures are almost the same that of clear sky conditions but the snow particle scattering effects are emphasized

To study the effect of LWP on the channels involved in the algorithm, the ratio of the brightness temperature depression to the LWP ( $\Delta T_B/LWP$ ), where  $\Delta T_B = T_{89} - T_{150}$ , is used (figure 14). The sensitivities increase with LWP as an exponential function. Although the complete profile also contains liquid and solid precipitation, the scattering index behaviour both complete and only CLW profiles is very similar denouncing a large contamination of the cloud liquid water on the brightness temperature differences. It is worth noting that the overlap of two profiles around 300-500  $g/m^2$ , thereafter ( $500 g/m^2$ ) cloud liquid water content dominates the sensitivity parameter. By using a regression analysis on the synthetic dataset, a new offset equation for Bennartz scattering index over sea and based on the frequencies at 89 GHz and 150 GHz has been developed.

$$off_{sea} = 106.559^{[a(T_{89}-T_{150})+b]}$$

so that the (B2) became

$$s_{s1} = (T_{89} - T_{150}) - (-Off_{sea} + 0.1104\theta)$$

where  $a = 0.083647$  and  $b = -0.901631$ .

In figure 14 the brightness temperature offset sensitivities (red dots) applied to the complete profile is presented. The sensitivity decreases as an exponential function to low values of LWP, thereafter becoming small dependent on the LWP.

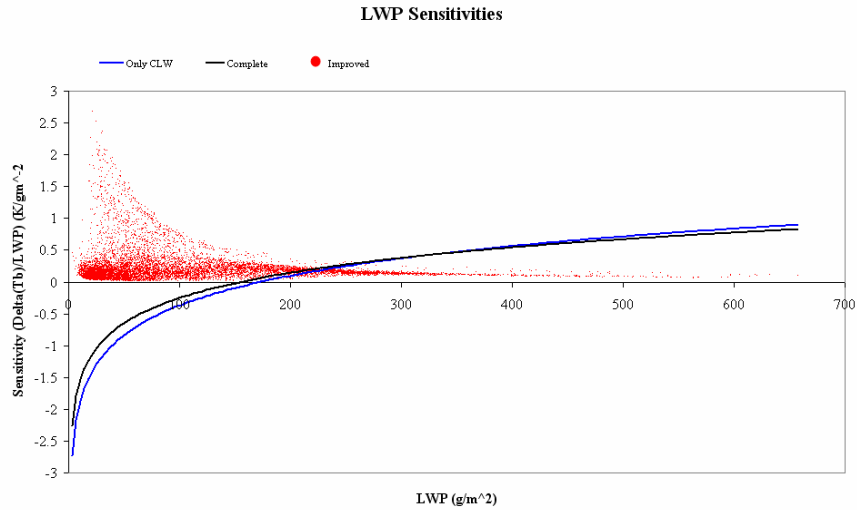


Fig. 14: Sensitivity versus LWP shows the exponential dependence of the  $\Delta T_B$  complete (blue) and only CLW (black) profiles. The  $Off_{sea}$  performance is in red dots.

The accreting effects of the cloud liquid water content can be seen in figures 15 and 16. In figure 15, a large part of scattering index signature ranges (10 to 50 K in circled area) used to evaluate rain rate intensities is affected by the cloud liquid water (pink dots). The scattering index values in the range 30-50 K are due to the presence of the liquid and solid rain particles in the profile. By using the brightness temperature offset  $Off_{sea}$ , low effect of the cloud liquid water with respect to the rain signature is obtained preserving rainy signal.

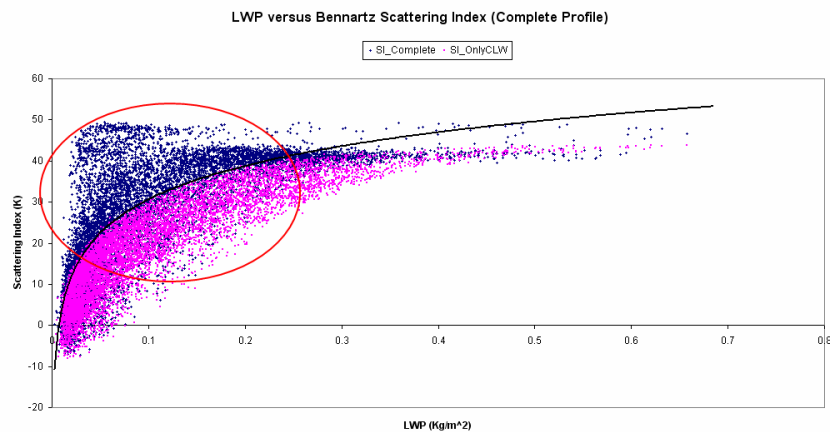


Fig. 15: Scattering Index signatures with fixed offset threshold applied to the complete profile (blue) and only CLW (pink). CLW signature affects the scattering index signal in the range 10-50 K (circled area) used in the rain rate estimations

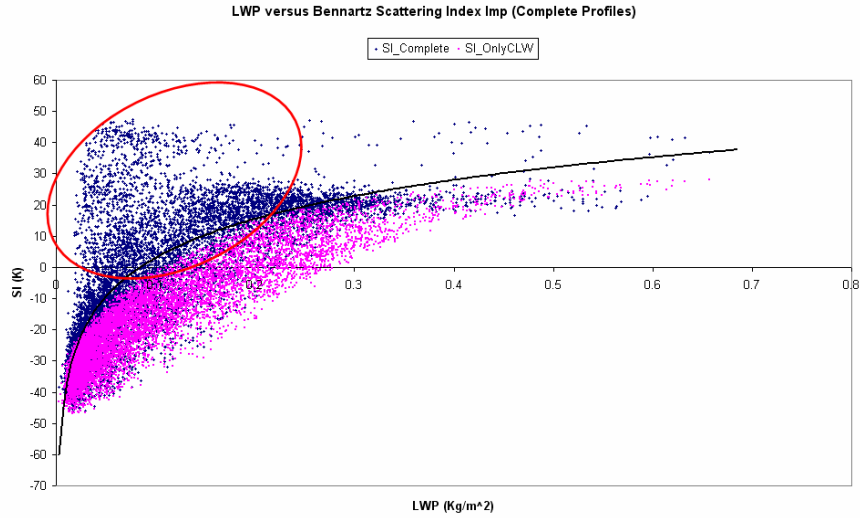


Fig. 16: Scattering index with  $Off_{sea}$  applied to complete profile (blue) and only CLW (pink). With respect to the fixed threshold, the scattering signal is mainly due to the snow and rain

The brightness temperature offset,  $Off_{sea}$ , on the same case studies considered above has been applied. The Bennartz algorithm with  $Off_{sea}$  is more comparable to the radar data than with the constant offset threshold. Particularly, this can be seen in the figure 19 (top-left), where a value of 30 K is computed on the radar free-precipitation areas. Nevertheless, the new offset threshold is not perfect because some precipitating areas detected to the radar are classified as free-precipitation pixels.

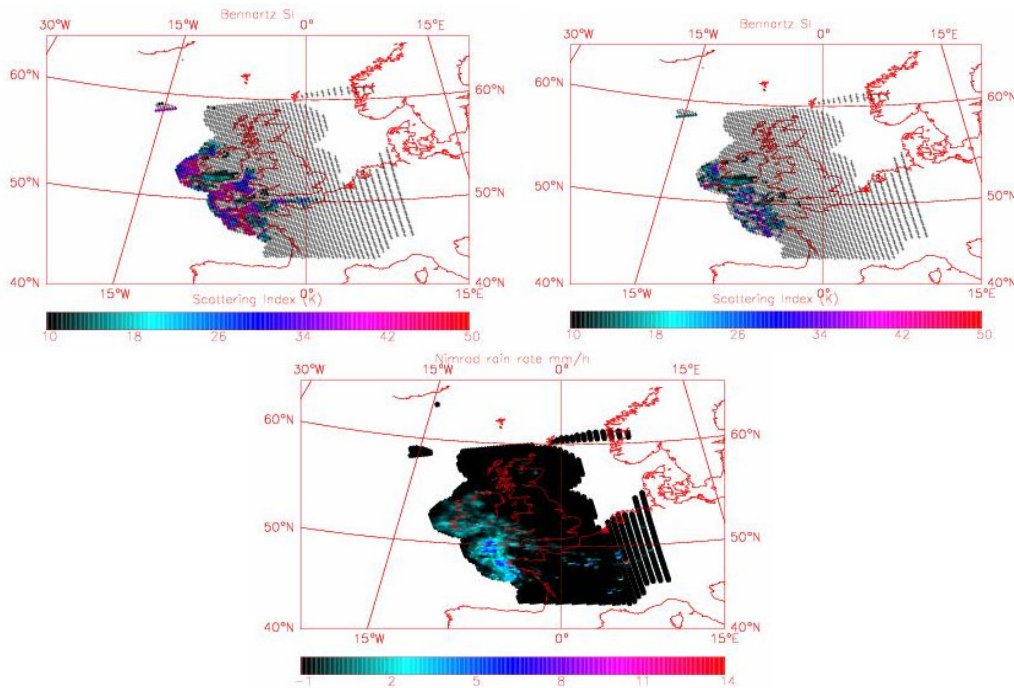


Fig. 17: Scattering index fixed threshold (top-left), improved scattering index threshold (top-right) and co-located radar data (bottom) at 1400 on 22/06/04, convolved to the AMSU-B grid

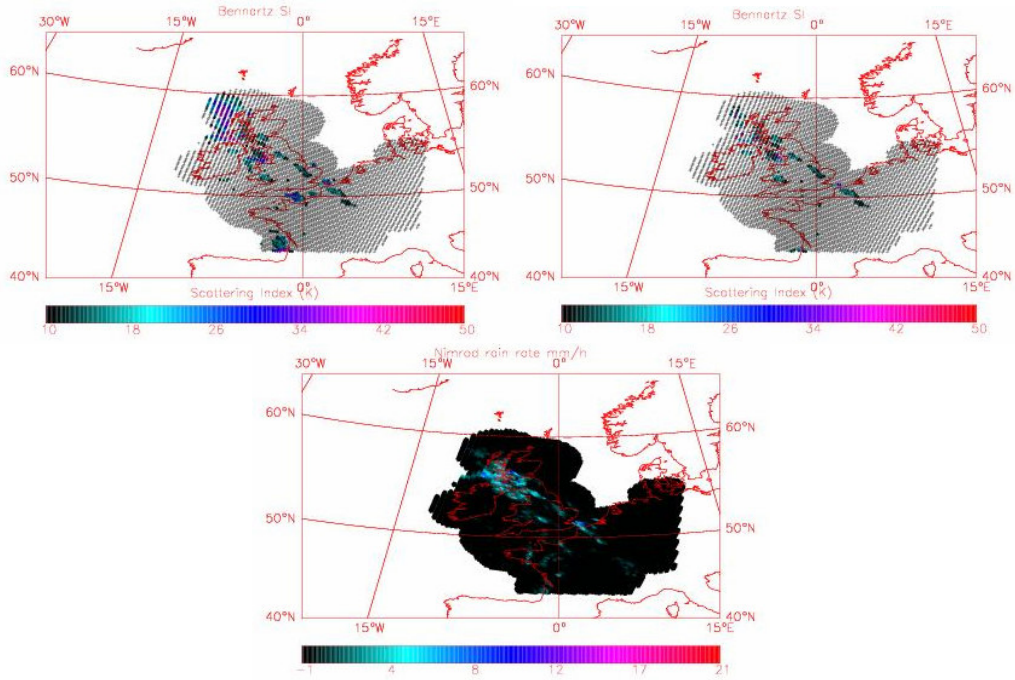


Fig. 18: Scattering index fixed threshold (top-left), improved scattering index threshold (top-right) and co-located radar data (bottom) at 0700 on 09/008/04, convolved to the AMSU-B grid

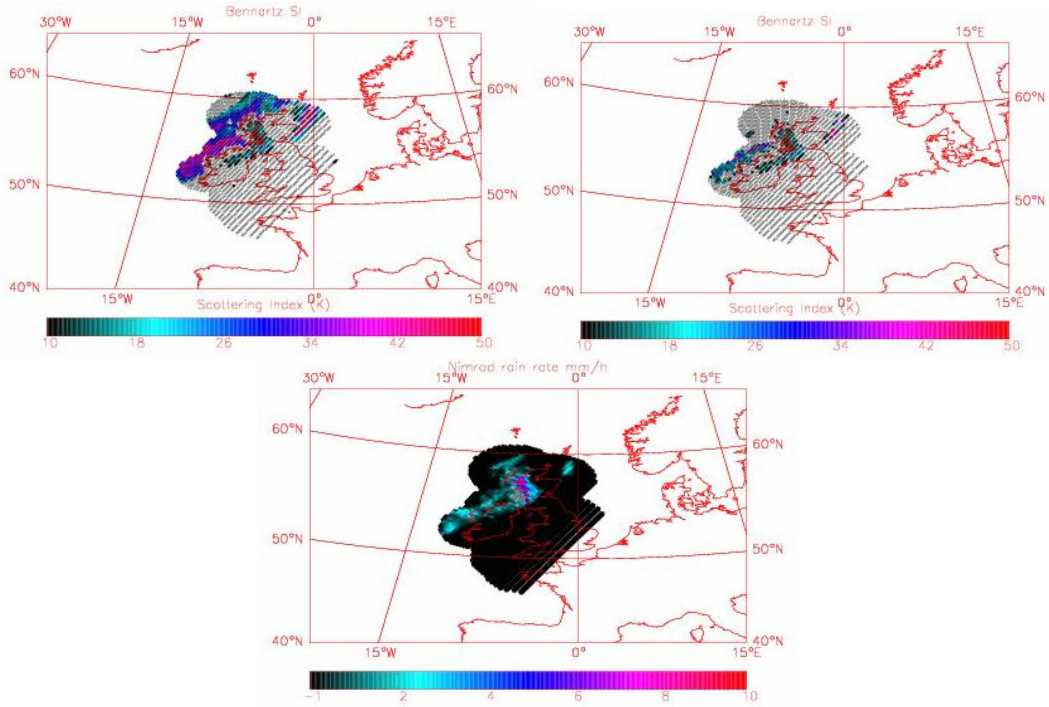


Fig. 19: Scattering index fixed threshold (top-left), improved scattering index threshold (top-right) and co-located radar data (bottom) at 0430 on 12/12/04, convolved to the AMSU-B grid

## 6. Summary and Conclusions

In this report, I describe a work devoted to calculate a new brightness temperature offset in order to improve the Bennartz scattering index approach over the ocean surface. The approach suggested by Bennartz of the classes of precipitation intensities was used. To understand not only the strengths and weaknesses of the Bennartz technique, already emphasized in [10], but also to evaluate the performance with a different algorithm to derive precipitation rates, the first step was to compare two different techniques: the Bennartz and Grody algorithms. The qualitative comparisons show as the Bennartz scattering indices are closer to the radar data than for Grody, particularly over water surface. The latter question has been emphasized by quantitative analysis showing a good match between two techniques over land surface but not over sea. Nevertheless, since the Bennartz equations are affected by the increasing cloud liquid water a new offset brightness temperature is used to improve the scattering index over sea surface.

By using ECMWF profiles over ocean surface, AMSU-B brightness temperatures have been simulated in order to evaluate the effects of each parameter on AMSU-B window channels. Two interesting aspects are picked out. First, the absorption at 89 GHz due to the cloud liquid water is very large compared to 150 GHz and with respect to the other parameters. Consequently, the scattering index in presence of large amount of liquid water path overestimates the rain intensity, particularly with scattering particles which greatly reduce the signal at 150 GHz.

Therefore, a new brightness temperature offset has been computed to reduce the LWC effects on the rain evaluations. The equation (B2) with the new offset, has been applied to the North-Europe and UK areas giving best results compared to the fixed offset.

Although these results are encouraging, further investigations of new offset threshold capabilities in the regions where, both climate conditions and precipitation types are different, are needed.

## References

- [1] Grody N., Weng F. and Ferraro R., 2000: Application of AMSU for obtaining hydrological parameters. *6<sup>th</sup> Specialist meeting on Microwave Radiometry and Rem. Sens. of the Environ., USP Int. Science Publishers*, 16-18 March 99, Florence, Italy.
- [2] Staelin D. H. and Chen F., "Precipitation observations near 54 and 183 GHz using the NOAA-15 satellite", *Geoscience and Remote Sensing*, vol. 38, no. 5, 2322-2332, 2000
- [3] Deidda R., Benzi R. and Siccardi F. "Multifractal modelling of anomalous scaling laws in rainfall ", *Water Resources Research*, vol. 35 no. 6, 1853-1867 , 1999
- [4] Deidda R., "Rainfall downscaling in space-time multifractal framework ", *Water Resources Research*, vol. 36 no. 7, 1779-1794, 2000
- [5] Bennartz R, A. Thoss and D.B. Michelson : "Precipitation analysis using the Advanced Microwave Sounding Unit in support of Nowcasting Application ", *Metorol. Appl.* vol. 9, 177-189, 2002
- [6] Zhang G. Vivekanandan J. and Politovich M.K., "Scattering Effect on Microwave Remote Sensing of Cloud Parameters", Preprints, 8<sup>th</sup> Conference on Aviation, Range, and Aerospace Meteorology, AMS, Dallas Texas, 497-501, 1999
- [7] Evans F. and Stephens G. L., "Microwave radiative transfer through clouds composed of realistically shaped ice crystals. Part I: single scattering properties ", *Journal of the Atmospheric Science*, vol. 52, no. 11, 2041-2057, 1995
- [8] Evans F. and Stephens G. L., "Microwave radiative transfer through clouds composed of realistically shaped ice crystals. Part II: single scattering properties ", *Journal of the Atmospheric Science*, vol. 52, no. 11, 2041-2057, 1995
- [9] Bennartz R., Thoss A. and Fisher J., "Retrieval of Microwave Precipitation and Columnar Water Vapour Path from AMSU A/B", *Proc. IX TOVS Study Conference, Igls, Austria*, 20-26 February 1997, 11-20
- [10] O'Keeffe U., "Crisis area model precipitation imagery over all terrain", *Final Report*, May 2005